Non-collinear upconversion of infrared light

Pedersen, Christian; Hu, Qi; Høgstedt, Lasse; Tidemand-Lichtenberg, Peter; Dam, Jeppe Seidelin

Published in:
Optics Express

Link to article, DOI:
10.1364/OE.22.028027

Publication date:
2014

Document Version
Publisher's PDF, also known as Version of record

Non-collinear upconversion of infrared light

Christian Pedersen, Qi Hu, Lasse Høgstedt, Peter Tidemand-Lichtenberg, and Jeppe Seidelin Dam*

DTU Fotonik, Frederiksborgvej 399, 4000 Roskilde, Denmark
jdam@fotonik.dtu.dk

Abstract: Two dimensional mid-infrared upconversion imaging provides unique spectral and spatial information showing good potential for mid-infrared spectroscopy and hyperspectral imaging. However, to extract spectral or spatial information from the upconverted images an elaborate model is needed, which includes non-collinear interaction. We derive here a general theory providing the far field of the upconverted light when two arbitrary fields interact inside a nonlinear crystal. Theoretical predictions are experimentally verified for incoherent radiation and subsequently applied to previously published data with good agreement.

OCIS codes: (110.3080) Infrared imaging; (190.7220) Upconversion; (300.6340) Spectroscopy, infrared.

References and links

1. P. R. Griffiths and J. A. de Haseth, *Fourier Transform infrared Spectrometry 2nd Ed* (Wiley, 2007).
2. S. Wartewig and R. H. H. Neubert, "Pharmaceutical applications of mid-IR and raman spectroscopy," Adv. Drug Deliver. Rev. ***57(8)***, 1144–1170 (2005). ***http://www.sciencedirect.com/science/article/pii/S0165993602012086***
3. N. B. Colthup, L. H. Daly, and S. E. Wiberley, *Introduction to Infrared and Raman Spectroscopy 3rd ed.* (Academic 1990).
4. T. L. Williams, *Thermal Imaging Cameras* (CRC, 2009).
5. J. E. Midwinter, "Image conversion from 1.6um to the visible in lithium niobate," Appl. Phys. Lett. **12**(3), 68–71 (1968), doi:10.1063/1.1651902.
6. J. S. Dam, C. Pedersen, and P. Tidemand-Lichtenberg, "Room-temperature mid-infrared single-photon spectral imaging," Nature Photon. **6**, 788 (2012). *http://www.nature.com/doifinder/10.1038/nphoton.2012.231*
7. Q. Zhou, K. Huang, H. Pan, E. Wu, and H. Zheng, "Ultrasensitive mid-infrared up-conversion imaging af few-photon level," Appl. Phys. Lett. **102**(24), 241110 (2013), doi:10.1063/1.4811826.
8. J. S. Dam, C. Pedersen, and P. Tidemand-Lichtenberg, "High-resolution two-dimensional image upconversion of incoherent light," Opt. Lett. **35**(22), 3796–3798 (2010), doi:10.1364/OL.35.003796.
9. C. Pedersen, E. Karamehmedović, J. S. Dam, and P. Tidemand-Lichtenberg, "Enhanced 2D-image upconversion using solid-state lasers," Opt. Express **17**(23), 20885–20890 (2009), http://www.opticsinfobase.org/oe/abstract.cfm?URI=oe-17-23-20885.
10. J. S. Dam, C. Pedersen, and P. Tidemand-Lichtenberg, "Theory for upconversion of incoherent images," Opt. Express **20**(2), 1475–1482 (2012), http://www.opticsinfobase.org/oe/abstract.cfm?URI=oe-20-2-1475.
11. N. Bloembergen and P. S. Pershan, "Light waves at the boundary of nonlinear media," Phys. Rev. **128**(2), 606–622 (1962), http://prola.aps.org/abstract/PR/v128/i2/p606_1.
12. D. A. Kleinman, "Theory of optical parametric noise," Phys. Rev. **174**(3), 1027–1041 (1968), http://prola.aps.org/abstract/PR/v174/i3/p1027_1.
13. A. H. Firester, "Upconversion: Part III," J. Appl. Phys. **41**(2), 703–709 (1970).
14. A. Gavrielides, P. Peterson, and D. Cardimona, "Diffractive imaging in three-wave interactions," J. Appl. Phys. **62**(7), 2640–2645 (1987).
15. B. E. A. Saleh and M. C. Teich, *Fundamentals of Photonics 2nd Ed* (Wiley, 2007).
16. J. W. Goodman, *Introduction to Fourier Optics 3rd Ed* (Roberts & Company, 2005).
17. Q. Hu, J. Seidelin Dam, C. Pedersen, and P. Tidemand-Lichtenberg, "High-resolution mid-IR spectrometer based on frequency upconversion," Opt. Lett. **37**(24), 5232–5234 (2012), http://www.opticsinfobase.org/ol/abstract.cfm?uri=ol-37-24-5232.
18. L. Høgstedt, O. B. Jensen, J. S. Dam, C. Pedersen, and P. Tidemand-Lichtenberg, "500 nm continuous wave tunable single-frequency mid-IR light source for C-H spectroscopy," Laser Phys. **22**(11), 1676–1681 (2012), doi:10.1134/S1054660X12110047.
19. The commercial HITEMP database from "Spectral calculator - high resolution gas spectra," *http://www.spectralcalc.com/*

#222035 - $15.00 USD Received 1 Sep 2014; revised 24 Oct 2014; accepted 28 Oct 2014; published 4 Nov 2014

1. Introduction

Highly sensitive mid-infrared (mid-IR) imaging and spectroscopy is emerging as an attractive alternative to its more well-known visible or near-infrared counterparts within fundamental band gas analysis, spectral identification and quantification of complex molecules [1–3].

Mid-IR detectors exist in different forms [4], but they are all limited by an unavoidable dark noise due to thermal radiation originating from the finite temperature of the detector itself [4]. Thus, high sensitivity mid-IR detectors need to be cooled to reduce noise. This is in strong contrast to visible (VIS) or near infrared (NIR) detectors where thermal radiation (dark noise) is much less pronounced at room temperature.

An attractive alternative to cryogenically cooled mid-IR detection and imaging is room-temperature frequency upconversion followed by detection in the VIS or NIR region [5–7]. This method relies on a two stage procedure. First, sum frequency generation (SFG) in a $\chi^{(2)}$ nonlinear crystal, converting the incoming mid-IR light into a shorter wavelength interval well below the wavelength range of thermal radiation emitted by room temperature objects. Second, NIR/VIS detection using highly sensitive silicon detectors or CCD cameras. With this approach, single photon mid-IR imaging can be accomplished [6]. Even high resolution images can be upconverted [8]. However, to understand and exploit the attractive features of upconversion, a more elaborate model of the image formation is needed. This is the primary scope of the present paper.

In [9,10] a model was developed for upconversion of coherent and incoherent radiation respectively, assuming small angles of incidence for the mid-IR light, i.e. nearly collinear interaction. In this work, the far field solution of the upconverted field is determined for arbitrary input field and pump beam respectively in the undepleted regime. The far field restriction imposed here leads to a particular simple description; however, if needed, near field solutions can be calculated as well. The important case of non-collinear interaction between a Gaussian pump beam and an incident plane wave at a large angle of incidence is considered thoroughly. This work can also be considered as an extension of [11] where SFG of three plane waves were treated [12], where spontaneously parametric down conversion was considered assuming plane input waves and a Gaussian pump beam, or [13, 14] which provide a detailed analysis of an arbitrary incident input field upconverted by a plane wave pump beam. We derive a theoretical expression for the upconverted image intensity distribution and spectral resolution, as a result of the finite spot size of the pump beam, i.e. the acceptance parameters of the nonlinear image upconversion process. The model is experimentally verified and found to be in good agreement with measurements. Finally, previous published results will be discussed and modeled using the developed theory.

2. Theory

The standard treatment of SFG found in the nonlinear optics literature, such as [15] relies on three coupled nonlinear differential Eqs. from which the detailed interaction of the three plane waves can be calculated including depletion. This study focuses on 2-dimensional upconversion imaging of faint objects where depletion is irrelevant; however, to describe imaging adequately a model including arbitrary input fields is needed including non-collinear interaction of the incident beams. Furthermore, we will mainly be interested in farfield solutions, although the suggested approach can be expanded to cover near field solutions of the upconverted field as well. Walk-off in the input fields is implicitly included in the model. However, the developed model does not specifically include walk-off of the upconverted field, but it can be extended to consider a constant walk-off by applying the walk-off in the opposite direction to both the input fields. With aforementioned assumptions, a particularly simple upconversion model can be developed. We adopt a general approach based on the far field solution to the Helmholtz Eq. in free space including a nonlinear source term [14] rather than a on a coupled set of differential Eqs. This approach, which shares common traits with

#222035 - $15.00 USD Received 1 Sep 2014; revised 24 Oct 2014; accepted 28 Oct 2014; published 4 Nov 2014

scattering theory, provides a simple direct treatment exploiting results found in the general electromagnetic theory, e.g [16]. Figure 1 shows the SFG process inside a nonlinear medium, V with two arbitrary monochromatic input fields expressed as par-axial waves, $E_1\left(\vec{r}\right)e^{-i\vec{k}_1\cdot\vec{r}}$ and $E_2\left(\vec{r}\right)e^{-i\vec{k}_2\cdot\vec{r}}$ with angular frequency, ω_1 and ω_2 respectively, generating a third plane SFG wave, $E_3\left(\vec{r}\right)e^{-i\vec{k}_3\cdot\vec{r}}$ in the far field. $\vec{k}_1$ and $\vec{k}_2$ can be envisioned as spatial carrier frequencies specifying the "average" direction of the two incident fields respectively.

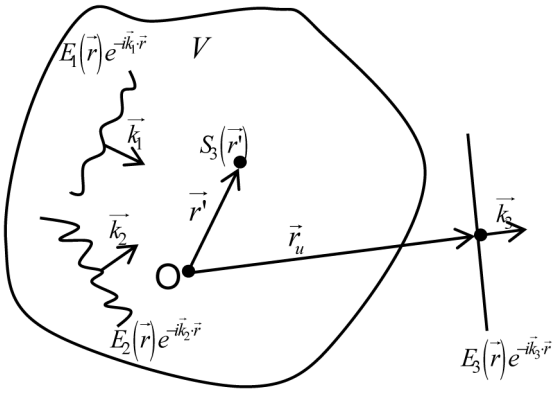

Fig. 1. General layout of sum frequency generation illustrating two arbitrary input fields inside a second order nonlinear material, V, generating a plane wave at the sum frequency in the far field.

The free space, far field solution to Helmholtz Eq. including nonlinear source terms can be expressed as [14,15], Eq. (1);

$$E_3\left(\vec{r_u}\right) \equiv E_3(r_u,\vec{k_3}) = \frac{\exp\left(-ik_3\cdot r_u\right)}{4\pi r_u}\int_V S_3\left(\vec{r'}\right)\exp\left(i\vec{k_3}\cdot\vec{r'}\right)dr' \qquad (1)$$

where V is the volume of the nonlinear material, and $\vec{r}_u$ is the far field observation point, $r_u = \left|\vec{r_u}\right|$ and $\vec{k}_3$ is the wave vector of the plane upconverted far field parallel to $\vec{r}_u$, see Fig. 1. The source term, $S_3\left(\vec{r'}\right)$, for a second order nonlinear interaction process is given by [15], Eq. (2);

$$S_3\left(\vec{r'}\right) = -\frac{\partial^2 P}{\partial^2 t} = -2\frac{d_{eff}\omega_3^2}{c^2}E_1\left(\vec{r'}\right)E_2\left(\vec{r'}\right)e^{-i(\vec{k}_1+\vec{k}_2)\cdot\vec{r'}} \qquad (2)$$

where $\omega_3 = \omega_1 + \omega_2$ is the angular frequency of the upconverted field, $E_3\left(\vec{r}\right)$ induced via the second order nonlinear response of the two incident electrical fields, $E_1\left(\vec{r}\right)$ and $E_2\left(\vec{r}\right)$, c is the speed of light in vacuum and d_{eff} is the effective second order nonlinear coefficient.

We observe from Eq. (1), that we indeed have a plane wave in the far field in the direction of $\vec{k}_3$. Two distinct assumptions are introduced in Eq. (1), the first is the 1st Born approximation and the second is that only far field solutions are considered, i.e. that the observation point is far away relative to the dimensions of the volume, V. The far-field

#222035 - $15.00 USD Received 1 Sep 2014; revised 24 Oct 2014; accepted 28 Oct 2014; published 4 Nov 2014

approximation implies that $\overrightarrow{k_3}$ is the same for all points in the crystal. Hence, the approach can be applied even without assumption of uniform n_3.

If needed, the far-field approximation can be removed at this point using a more general solution to Helmholtz Eq [15,16], thus providing the near field solution in integral form.

Inserting Eq. (2) into (1) provides a compact and simple expression for the plane SFG far field, $E_3(r_u, \overrightarrow{k_3})$ specified by the wave vector, $\overrightarrow{k_3}$ and distance, r_u from the observation point;

$$E_3(r_u, \overrightarrow{k_3}) = -2\frac{d_{eff}\omega_3^2}{c^2}\frac{e^{-ik_3 r_u}}{4\pi r_u} F\left\{E_1\left(\vec{r}\right)\right\} \otimes F\left\{E_2\left(\vec{r}\right)\right\} \tag{3}$$

The Fourier transforms, $F\{\ \}$ in Eq. (3) are evaluated with the spatial frequencies, $\frac{\overrightarrow{-\Delta k}}{2\pi}$ inserted, where $\overrightarrow{\Delta k} \equiv \overrightarrow{k_3} - \overrightarrow{k_2} - \overrightarrow{k_1}$. In conclusion, the solution to Helmholtz Eq. in the far field is the Fourier transformation of the nonlinear induced field inside the volume of the nonlinear material. Note that this approach generalizes to other nonlinear processes like four-wave mixing. Note that $\overrightarrow{\Delta k}$ in general has three non-zero components and may point in any direction; in the special case of plane wave interaction inside a nonlinear crystal of infinite transverse dimensions, the transverse components of $\overrightarrow{\Delta k}$ vanish [12], thus $\overrightarrow{\Delta k}$ becomes a scalar quantity. A proper explanation of this simplifying assumption is often lacking in literature.

2.1 A Gaussian pump beam and plane wave upconversion

Equation (3) can be evaluated analytically in the important case of a Gaussian pump field and an incident plane wave, see also Fig. 2. This simple case is chosen due to its relevance for the subsequent sections. The pump field is assumed to propagate along the *z*-axis, having a Gaussian beam profile with beam waist, w_0 at $z = 0$, wavelength, λ_2 and wave number, k_2 [12], Eq. (4);

$$E_2\left(\vec{r}\right)\exp\left(-ik_{2z}z\right) = \frac{a_2}{1+i\frac{z}{z_R}}\exp\left(-ik_{2z}z\right)\exp\left(-\frac{x^2+y^2}{w_0^2\left(1+i\frac{z}{z_R}\right)}\right), \tag{4}$$

where $z_R = \frac{k_{2z}w_0^2}{2}$ and a_2 is the field amplitude of the linearly polarized pump laser. The incident field is given as a plane wave. Equation (5) uses the notation shown in Fig. 1 to explicitly emphasize the carrier wave vector component of the incident field, Eq. (5);

$$E_1\left(\vec{r}\right)\exp\left(-i\overrightarrow{k_1}\cdot\vec{r}\right) = a_1\exp\left(-i\overrightarrow{k_1}\cdot\vec{r}\right), \tag{5}$$

where a_1 is the electric field amplitude and $\overrightarrow{k_1}$ is the corresponding wave vector. Inserting Eq. (4) and Eq. (5) into Eq. (3) yields;

$$E\left(r_u, \Delta k_x, \Delta k_y, \Delta k_z\right) = 2\frac{d_{eff}\omega_3^2\pi w_0^2 l}{c^2}\frac{e^{-ik_3 r_u}}{4\pi r_u}a_1 a_2 e^{-\frac{\left(\Delta k_x^2+\Delta k_y^2\right)w_0^2}{4}}\,\mathrm{Sin\,c}\left(\frac{l}{2}\left(\Delta k_z - \frac{\left(\Delta k_x^2+\Delta k_y^2\right)}{2k_{2z}}\right)\right) \tag{6}$$

#222035 - $15.00 USD Received 1 Sep 2014; revised 24 Oct 2014; accepted 28 Oct 2014; published 4 Nov 2014

From Eq. (6) it is seen $(\Delta k_x, \Delta k_y)$ relate to the deviation from conservation of transverse momentum, i.e. the point spread function in the imaging process. We note that this result corresponds well with [12] where the special case of spontaneous parametric down conversion was analyzed. Also note that the Gouy phase shift is included, known to slightly shift the optimal phase match condition for focused beams.

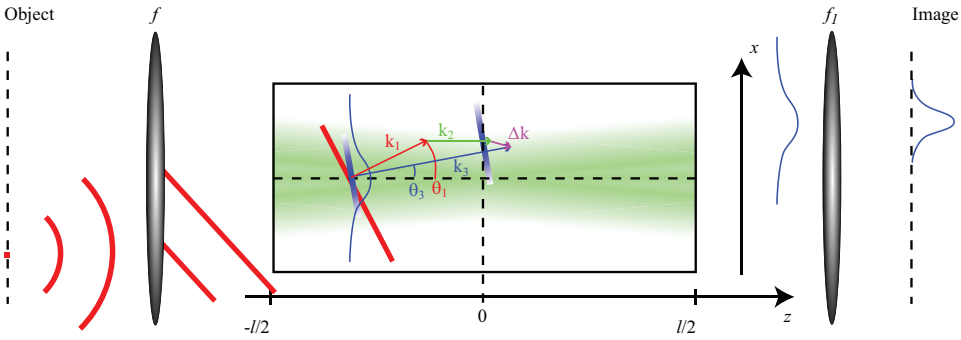

Fig. 2. Illustration of the non-linear crystal, the object and image planes respectively and the three wave-vectors involved in the non-collinear interaction.

In a practical realization the far field condition of the upconverted beam can be met by including a Fourier transforming lens with focal length, f_1. See Fig. 2. Similarly, a first Fourier transforming lens, with focal length f, transforms points in the object plane into hereto unique angles inside the nonlinear crystal. Incident polychromatic light from a real object can then be modeled as a plurality of plane waves.

In the following one such incident plane wave is considered. For the incoherent case, the intensity profile at the image plane is obtained from Eq. (6) replacing E fields with intensities and spectral radiance [16], transforming angular coordinates to positions, and finally impose proper correspondence to earlier published quasi-collinear theory [10] using a proper scaling factor. The result is Eq. (7);

$$I_{image}\left(\vec{r_u},\lambda_3\right)=\frac{8\pi^2 d_{eff}^2 l^2 P_{Gauss}}{n_1 n_2 n_3 \varepsilon_0 c \lambda_3^2 f^2}$$

$$\times\int L_{object}\left(\vec{r''},\lambda_1\right)\left(\frac{w_0^2 k_3^2}{2\pi n_3^2 f_1^2} e^{-\frac{w_0^2 k_3^2 \left|\vec{r_u}-\vec{r''}\right|^2}{2n_3^2 f_1^2}} \operatorname{sinc}^2\left(\frac{l}{2}\left(\Delta k_z\left(r'',r_u\right)-\frac{k_3^2}{2k_2}\frac{\left|\vec{r_u}-\vec{r''}\right|^2}{n_3^2 f_1^2}\right)\right)\right) d\vec{r''}, \quad (7)$$

where $\vec{r_u}=(x_u,y_u)$ is the coordinates of a point in the image plane and $\vec{r''}=-\frac{\lambda_3 f_1}{\lambda_1 f}\vec{r}$, where $\vec{r}$ is a coordinate in the object plane. f is the focal length of the 2f lens Fourier transforming the object plane to the nonlinear crystal. $\Delta k_z\left(r'',r_u\right)$ is calculated from $\Delta k_z\left(r,r_u\right)=k_3\cos\left(\theta_u\right)-k_2-k_1\cos\left(\theta_i\right)$, where θ_i and θ_u are the internal crystal angles of the incident and upconverted field, $\theta_i\approx\frac{r}{n_1 f}$ and $\theta_u\approx\frac{r_u}{n_3 f_1}$ respectively. ε_0 is the vacuum permeability. $L_{object}\left(\vec{r},\lambda_1\right)$ is the spectral radiance of the object and P_{Gauss} is the power of the Gaussian pump beam. Equation (7) expresses image upconversion including non-collinear interaction needed for describing the image formation. The expression includes diffraction of both the upconverted field and the laser beam. The point where the non-collinearity becomes

#222035 - $15.00 USD Received 1 Sep 2014; revised 24 Oct 2014; accepted 28 Oct 2014; published 4 Nov 2014

important is related to the angle of the upconverted field, θ_u, i.e. the radial position in the image plane, so that quasi-collinear performance is maintained for upconverted internal angles significantly smaller than $\sim w_0/l$. Equation (6) and Eq. (7) provide the basic Eqs. for calculation of the acceptance parameters. The actual evaluation of Eq. (7) generally requires a numerical computation. In the following section examples of such calculations are presented and compared against experimental data.

3. Comparison to experimental data

In this section, the developed model, i.e. Equation (7), is first compared against experimental results and subsequently applied to previously published experimental data as presented in [17]. To illustrate the impact of a finite pump beam size on the upconverted intensity distribution, a numerical calculation of the upconverted intensity using a 180 µm pump beam size is compared to that of a very large pump beam diameter. The calculation is performed for fixed wavelengths, $\lambda_1 = 2.937\,\mu\text{m}, \lambda_2 = 1.064\,\mu\text{m}$ and $\lambda_3 = 0.781\,\mu\text{m}$ varying the phase match condition through use of different poling periods. In order to reduce the numerical complexity, the model is reduced to two dimensions (x,z). The normalized intensity distribution from the object is modelled as constant in $\vec{r}$, i.e. uniform light emission. In the following calculations, all angles will be presented as internal crystal far field angles, θ_u i.e. not including refraction of the light at the crystals interface. The blue graphs in Fig. 3(a) shows the normalized intensity for a very large Gaussian pump spot size at 11 different phase match conditions, whereas the red graphs shows the corresponding intensities for a 180 µm Gaussian pump beam. The graph in Fig. 3(b) shows the decreasing peak intensity for increasing angles when using a 180 µm pump beam spot size, i.e. it represents how the monochromatic peak intensity decreases for larger phase matched angles. It is important to note that the shape of the curve is independent of the choice of wavelengths, w_0, and L. In all circumstances the curve drops to about 0.5 at the point $\theta_u = w_0/L$ as indicated in Fig. 3(b).

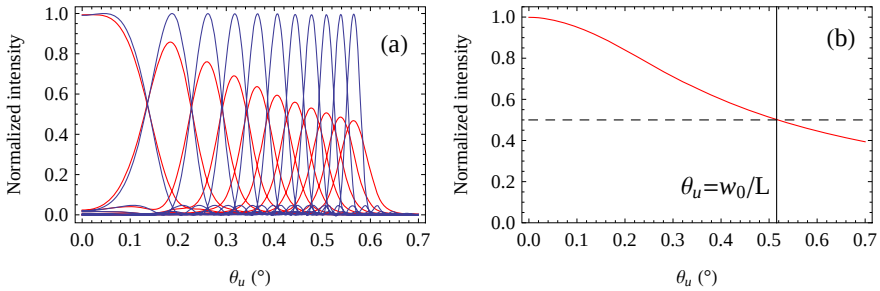

Fig. 3. Theoretical calculation of of non-collinear upconversion of monochromatic incoherent light. a) The blue curves shows the normalized intensity curves for a very large laser beam diameter for a selection of phase matched angles; θ_u = 0.046, 0.187, 0.262, 0.318, 0.365, 0.406, 0.444, 0.478, 0.509, 0.538, and 0.565 degrees respectively. The red curves shows a similar set of curves using a pump beam radius of 180 µm. b) This curve shows the decreased peak intensity values caused by the finite size of the mixing beam as a function of non-collinear upconverted angle.

To calculate the spectral response, we now assume that the spectral radiance from the object is constant in λ_1 and $\vec{r}$. The phase matched upconverted wavelength is still λ_1 = 2.937 µm, corresponding to an upconverted wavelength λ_3 = 0.781 µm. The result is shown in Fig. 4, where each curve corresponds to the same phase matched angles used in Fig. 3, again showing decreasing peak conversion efficiency for increasing angle.

#222035 - $15.00 USD Received 1 Sep 2014; revised 24 Oct 2014; accepted 28 Oct 2014; published 4 Nov 2014

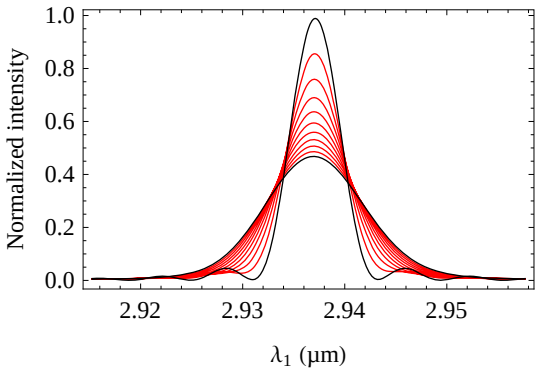

Fig. 4. Plot of spectral acceptance for the same angles θ_u used in Fig. 4(a). The highest curve shows the situation for the smallest angle, i.e. θ_u. As in Fig. 3, the absolute intensity peaks decrease for increasing θ_u. For easy comparison, the calculation uses the same phase matched wavelength. It is apparent that the decrease in peak intensity is accompanied with a corresponding increase in wavelength acceptance.

Figure 4 demonstrates that the spectral acceptance bandwidth increases for larger angles. This is a direct consequence of the finite pump beam radius in the upconversion process. Note that increasing the pump beam radius counteracts the increased acceptance bandwidth without decreasing the number of upconverted photons in case of incoherent light emission from the object [10, 12]. However, the laser beam size is ultimately limited by the nonlinear crystal aperture, particularly relevant when using periodically poled crystals. Thus for incoherent upconversion, high spectral (and spatial) resolution can be obtained with a large pump beam diameter.

3.1 spatially incoherent single frequency input

In order to test the developed theory, an experimental setup was established, see Fig. 5. The upconversion setup, described in detail in [17], uses a 20 mm long PP:LN crystal for sum-frequency mixing with a single-frequency 1064 nm pump beam with a beam size of 180 μm in the nonlinear crystal. The upconversion system is illuminated by spatially incoherent but monochromatic mid-IR light emitted from a single frequency mid-IR laser [18] scattered by a rotating diffuser.

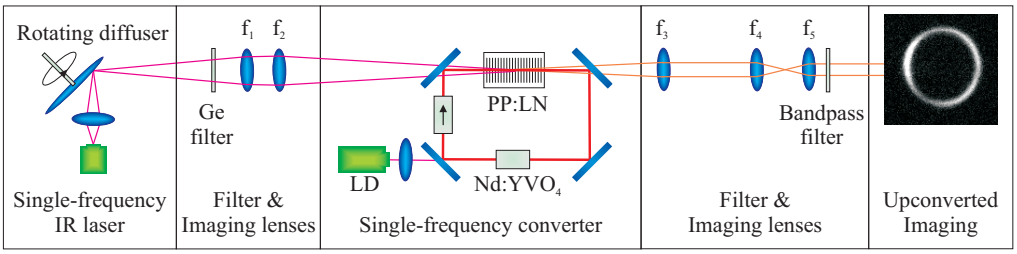

Fig. 5. System for detection of incoherent, monochromatic light using frequency up-conversion and a NIR/VIS CCD camera.

Figure 6(a) displays two raw data frames recorded with the CCD camera at different crystal temperatures. Upconverted incoherent single frequency input light will appear as a single unique ring pattern with varying radii as function of the temperature of the nonlinear crystal, i.e. changing the phase match condition [6]. Figure 6(b) shows the radial cross section curves of all the data frames recorded in the measurement series (5 frames of 100 ms exposure were averaged for each curve), corresponding to the graphs in Fig. 3, each

#222035 - $15.00 USD Received 1 Sep 2014; revised 24 Oct 2014; accepted 28 Oct 2014; published 4 Nov 2014

compared against theoretical curve using Eq. (7) (red graphs). Note that the phase match curves in Fig. 6(b) have been normalized to unity due to unwanted spatial inhomogeneity in the light distribution related to an imperfect diffuser. The spatial inhomogeneity can be observed as a non-uniform intensity pattern in the upconverted ring in Fig. 6(a). As a consequence of the normalization, the decreasing peak intensity with angle, shown in Fig. 3(b), is not observable. Thus the angular dependency only displays itself through the angular acceptance. The measured curves are averaged from several images using the center of the ring pattern as the origin.

To quantify the predictive power of the presented theory, the correlation coefficient, C of the experimental (blue graphs) and theoretical data (red graphs) is calculated. C is calculated according to Eq. (8):

$$C = \frac{\int I_{meas}(\theta_u) I_{theory}(\theta_u) \theta_u d\theta_u}{\sqrt{\int I_{meas}(\theta_u) I_{meas}(\theta_u) \theta_u d\theta_u \int I_{theory}(\theta_u) I_{theory}(\theta_u) \theta_u d\theta_u}} \tag{8}$$

Note that Eq. (8) is expressed in polar coordinates. In Fig. 6(c), the correlation coefficient, C between the actual measured values and those calculated from using collinear theory [10] (red dots) and the here presented non-collinear theory (blue dots) respectively, is plotted as a function of the phase match angle. It is clear that the proposed non-collinear theory is superior to the theory proposed in [10], particularly as the angle, θ_u increases.

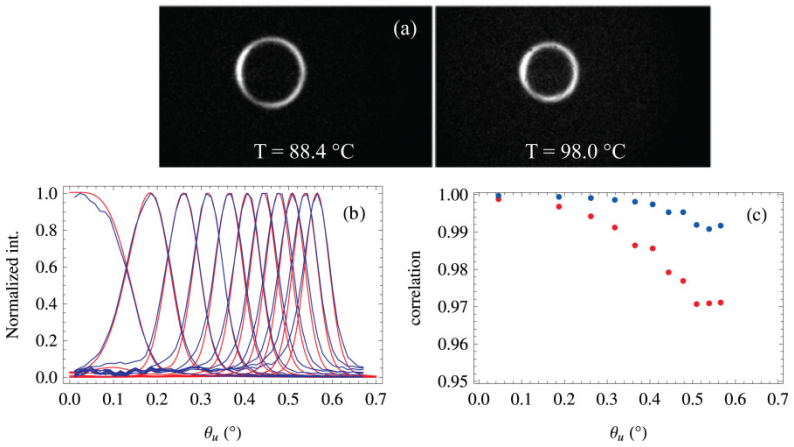

Fig. 6. Experimental comparison to theoretical prediction. a) Raw data recorded by the CCD camera for two different temperatures of the nonlinear crystal. b) Cross sections of the ring patterns as function of θ_u for different crystal temperatures (blue curves) plotted with theoretical predictions (red curves). The input wavelength was 2.937 μm throughout the measurement series. c) The correlation coefficient of the 11 data series comparing collinear theory (red dots) and non-collinear theory (blue dots).

3.2 Quasi-single frequency input

The developed theory for upconversion of incoherent quasi-single frequency light can also be applied to an input containing several frequencies. In work by Hu *et al.* [17], the emission lines of hot water vapor were studied based on upconversion followed by post filtering using a high finesse Fabry-Perot interferometer. In [17] the observed intensity decrease for increasing image angle was compensated using an empiric function rather than from theoretical considerations. With the here developed theoretical model, proper data correction can be applied. The result is shown in Fig. 7.

#222035 - $15.00 USD Received 1 Sep 2014; revised 24 Oct 2014; accepted 28 Oct 2014; published 4 Nov 2014

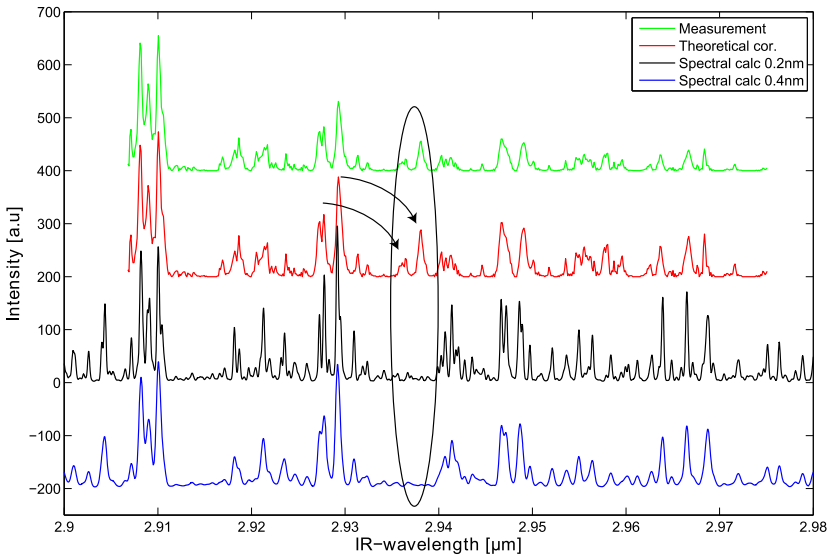

Fig. 7. The green curve shows the raw data from [17]. Post processing the green curve using the presented theory for non-collinear upconversion provides the red curve. The spectra are compared to a modelled spectra using [19] shown as black curve (0.2 nm resolution) and blue curve (0.4 nm resolution). The red curve resembles the modelled spectrum better as expected.

The here presented non-collinear theory is seen to partly explain the decrease in intensity when moving to larger image angles, i.e. wavelengths in this case. Regarding the spectral resolution, there is good agreement for the innermost part of the spectrum (around 2.91 μm). However, for the longer wavelengths a deteriorating spectral resolution is observed. This we believe to be caused by imperfect Fabry-Perot mirrors. The result is a decreased finesse for the off-center image locations, and thus reduced spectral resolution for the longer wavelengths. This can be observed by the resolution of the measurement series is matching the calculated spectrum at 0.2 nm resolution is matching experiments near 2.91 μm, whereas near 2.95 a better match is found when comparing to 0.4 nm resolution. A more detailed discussion of the decrease in spectral resolution observed in [17] is not central to this work. However, spectral artifacts in the measured spectrum when compared to the theoretically computed spectrum [19] can now be explained. These spectral artifacts appear as spectral signatures in wrong places for longer wavelengths, e.g. clearly visible at around 2.937 μm (marked by a circle in Fig. 7). From Fig. 4 we see that a free spectral range (FSR) of 9 nm is just enough to ensure monochromatic performance in the center of the image (highest black curve in Fig. 4), but for longer wavelengths, at off-center positions in the image, this is not the case (lowest black curve in Fig. 4). This causes the improper appearance of spectral artifacts shifted by 1 FSR.

4. Conclusion

In this work, a detailed theory is presented for the upconverted far field using two arbitrary input fields assuming no depletion. Directions are given how to include near field solutions as well. Equation (3) is a main theoretical result, whereas the solution in Eq. (7) enables simple computation for the incoherent case of a plane wave mixing with a Gaussian pump beam. The general theory developed here can be used to optimize the design of upconversion systems for future applications, and for improved post processing of measured data. In particular it is noted that for the incoherent case a large pump beam diameter favors both the spatial and the spectral resolution at no cost in efficiency.

The analytical model was experimentally verified showing good agreement with measured acceptance parameters for non-collinear interaction. The correction given by the roll-off curve

#222035 - $15.00 USD Received 1 Sep 2014; revised 24 Oct 2014; accepted 28 Oct 2014; published 4 Nov 2014

shown in Fig. 3(b) was applied to previous published experimental data improving the agreement with SpectralCalc simulations without the need for empirically correction as used in [17].

Acknowledgment

We thank Peter John Rodrigo for an interesting discussion on the theory presented here.

#222035 - $15.00 USD Received 1 Sep 2014; revised 24 Oct 2014; accepted 28 Oct 2014; published 4 Nov 2014